Hindawi Publishing Corporation
Advances in Astronomy
Volume 2012, Article ID 624987, 17 pages
doi:10.1155/2012/624987

Research Article

The Impact of Polarized Extragalactic Radio Sources on the Detection of CMB Anisotropies in Polarization

Marco Tucci[1] and Luigi Toffolatti[2, 3]

[1] *LAL, Université Paris-Sud and CNRS/IN2P3, 91400 Orsay, France*
[2] *Departamento de Física, Universidad de Oviedo, C. Calvo Sotelo s/n, 33007 Oviedo, Spain*
[3] *IFCA, Universidad de Cantabria, Avenida los Castros s/n, 39005 Santander, Spain*

Correspondence should be addressed to Marco Tucci, tucci@lal.in2p3.fr

Received 1 December 2011; Revised 21 March 2012; Accepted 2 April 2012

Academic Editor: Carlo Burigana

Recent polarimetric surveys of extragalactic radio sources (ERS) at frequencies $\nu \gtrsim 1$ GHz are reviewed. By exploiting all the most relevant data we study the frequency dependence of polarization properties of ERS between 1.4 and 86 GHz. For flat-spectrum sources the median (mean) fractional polarization increases from 1.5% (2–2.5%) at 1.4 GHz to 2.5–3% (3–3.5%) at $\nu > 10$ GHz. Steep-spectrum sources are typically more polarized, especially at high frequencies where Faraday depolarization is less relevant. Current data suggest that at high radio frequencies ($\nu \geq 20$) GHz the fractional polarization of ERS does not depend on total flux density and moderately increases with frequency. We estimate ERS number counts in polarization and the contribution of unresolved polarized ERS to angular power spectra. A first application is for the *Planck* satellite mission: we predict that only a dozen polarized ERS will be detected by the *Planck* LFI, and a few tens by the HFI. As for CMB power spectra, ERS should not be a strong contaminant to the CMB E-mode polarization at $\nu \gtrsim 70$ GHz, but they can become a relevant constraint for the detection of the cosmological B-mode polarization if the tensor-to-scalar ratio is $\lesssim 0.01$.

1. Introduction

The radiation emitted by extragalactic radio sources (ERS) at high radio frequencies, mainly synchrotron radiation from relativistic electrons in their jets and lobes, can be highly polarized, with an intrinsic degree of linear polarization as high as ∼70–75% in homogeneous sources with an unidirectional magnetic field (see, e.g., [1, 2], for comprehensive discussions on the subject).

These have to be considered as maximum values, which could be detected only in the case of very homogeneous sources with highly aligned magnetic field lines, which are unlikely to be observed among ERS. Actually, a much lower degree of total linear polarization, P, is commonly observed in ERS at cm or mm wavelengths (see e.g., [3, 4]), with only very few ERS showing a total fractional polarization, $\Pi = P/S$, as high as ∼10% of the total flux density, S.

Nevertheless, this low fractional polarization observed in ERS may constitute a problem for the detection of primordial polarization in the Cosmic Microwave Background (CMB), since ERS are the dominant polarized foreground at small angular scales and the CMB polarized signal is only a few percent of CMB temperature anisotropy. Therefore, CMB polarization studies need a careful determination of the polarized emission from foreground sources in general and of ERS in particular.

CMB polarized anisotropies can be decomposed into modes of even-parity (E-mode) and odd-parity (B-mode). As for the E-modes, generated by scalar perturbations in the primordial universe, they were first detected by [5] and all the following observations (e.g., [6, 7]) have confirmed measurements of CMB E-modes compatible with the concordance ΛCDM model. The more elusive B-modes are generated by tensor metric perturbations, that is, "primordial" gravitational waves generated during inflation, and, according to predictions of inflationary models, with an amplitude directly proportional to the energy scale at which the inflation occurred [8, 9]. A detection of these

"primordial" B-modes would provide the first real measure of the energy scale of inflation; thus, it would produce a real breakthrough in modern cosmology. But the detection of the B-modes CMB polarization—parameterized by the tensor-to-scalar ratio, $T/S = r$—is still a great challenge. In fact, the *Planck* mission [10, 11] (detailed discussions of the *Planck* Low Frequency Instrument (LFI) and High Frequency Instrument (HFI) expected polarization capabilities and calibrations are given by [12, 13]) would be marginally able to detect tensor metric perturbations by the direct detection of the primordial CMB B-mode, but only in the case of very high values of the tensor-to-scalar ratio of primordial perturbations, $r \gtrsim 0.05$–0.1 [14]. Otherwise, we will have to rely on proposed future space experiments, like COrE [15], specifically designed to detect CMB polarization by virtue of a much higher sensitivity than current ones.

The above discussion clearly illustrates the importance of giving the best up-to-date estimate of the average/median fractional polarization as well as of the distributions of fractional polarization [16], Π_i, at least for each one of the different ERS populations [17–19] which are providing relevant contributions to temperature anisotropies of the CMB.

Statistical studies of polarized emission from ERS have shown that at $\sim$1.4–5 GHz, the fractional polarization, Π, increases with decreasing flux density [3, 16, 20–22]. Different explanations have been proposed of this result, for example, a population change at fainter flux density [20, 22] or a changing fraction of radio-quiet AGN [3]. However, the cause of this increase in Π is still unknown. On the other hand, it has been shown by [16] that this increase of the degree of polarization with decreasing flux density is only observed, at cm wavelengths, for steep-spectrum ERS, that is, sources with $\alpha < -0.5$ if $S(\nu) \propto \nu^{\alpha}$, and not for flat-spectrum ERS ($\alpha \geq -0.5$).

Other very recent studies of the polarized emission in ERS have tried to analyze the dependence of the fractional polarization with luminosity, redshift, and the source environment. The current, still preliminary, results show no correlation between the fractional polarization and redshift, whereas a weak correlation is found between decreasing luminosity and increasing degree of polarization [23]. According to the analysis of highly polarized elliptical galaxies [24] no differences have been found in the source environments between low polarization and ultrahigh polarization sources. This result should indicate that a high polarization must be a result of intrinsic properties of ERS.

The outline of the paper is as follows: in Section 2 we briefly summarize the main processes giving rise to linear and circular polarization in ERS; in Section 3 we present current published data on the polarized emission from ERS; Section 4 is dedicated to discuss our current results on statistical properties of the polarized emission in ERS; in Section 5 we give a short review on the most recent cosmological evolution model for ERS; Section 6 presents our predictions on the contributions of ERS polarized radiation, given by unresolved sources, to the E- and B-modes; finally, in Section 7, we present our conclusions.

2. Polarized Emission from ERS

Observations as well as statistical studies of the fractional polarization of ERS are very interesting on their own, and not only because ERS constitute a major contaminant of the CMB polarized signal. In fact, they are an important tool in active galactic nuclei (AGN) research, as they give valuable information on the physical quantities which determine the characteristics of the synchrotron radiation emitted by relativistic electrons accelerated by homogeneous and/or random magnetic fields in AGN [1, 2].

On the one hand, precise measurements of the total synchrotron radiation emitted by a radio source give an estimate—under some assumption, that is, equipartition between the field and particle energy—of the total magnetic field strength. On the other hand, the degree of polarization of the radio wave provides information on the direction of the main magnetic field in the source environment and also on its degree of ordering. The magnetic field structure can, in turn, provide information on the relationship between the environments of the ERS and their properties.

As already noted, compact ERS typically show a degree of total linear polarization of a few percent of their radio total intensity. Therefore, magnetic fields in radio sources are believed to be highly inhomogeneous, or almost without ordering, although the observed nonvanishing linear polarization gives an indication of a certain degree of ordering of the field [25, 26].

The precise orientation of magnetic fields lines inside jets and lobes is still unknown, but theoretical arguments as well as observational evidence show that magnetic fields are indeed partially ordered. As for observations, these conclusions are based on measurements of the orientations of the linear polarization, revealing coherent structures across the images. From the theoretical point of view, an ordered magnetic field is expected when shocks compress an initially random field (with the field **B** perpendicular to the jet axis) or when such initial fields are sheared to lie in a plane, with **B** parallel to the jet axis [27–30].

Circular polarization (CP), which is a common feature of quasars and BL Lacertae objects (or simply BL Lacs), commonly known as blazars, (blazar sources are jet-dominated extragalactic objects—observed within a small angle of the jet axis—in which the beamed component dominates the observed emission [31]), is preferentially generated near synchrotron self-absorbed jet cores and is detected in about 30%–50% of these sources [25, 32]. In these inhomogeneous, optically thick, synchrotron sources, the emission of the electron population at lower energies is hidden by self-absorption. These invisible electrons produce *Faraday rotation* and conversion, which is the most likely mechanism capable of creating the observed CP in blazar sources [26, 32]. In any case, the measured degrees of CP are generally well below the levels of linear polarization [33], and thus negligible, at least at GHz frequencies.

The change in the position angle of the linearly polarized radiation which passes through a magnetoionic medium, that is, the *Faraday rotation*, can be expressed by the rotation angle $\Delta\phi[\mathrm{rad}] = \mathrm{RM}[\mathrm{rad/m^2}]\ \lambda^2[\mathrm{m^2}]$ [26, 34] experienced

by the polarization vector, where RM indicates the *rotation measure*. The rotation measure, RM, is the line-of-sight integral $\mathrm{RM}[\mathrm{rad}/m^2] = 0.81 \int n_e[\mathrm{cm}^{-3}] B_{\parallel}[\mu G] d\ell[\mathrm{pc}]$, n_e being the electron density and $B_{\parallel}$ the component of the magnetic field along the line-of-sight [35].

If the rotation depth is the same for all the emission volumes of the radio source, the net result is a rotation equal to RM λ^2 of the direction of polarization, without any effect on the degree of polarization. To change the degree of polarization there must be a variation in depth, either along or transverse to the line-of-sight [26].

Faraday rotation is commonly observed towards extragalactic radio sources. It was first observed by [36], who found an RM of -60 rad/m^2 towards the center of Centaurus A. More recently, observations of the rest-frame RM in AGN cores and jets reported values from a few hundreds to several thousands rad/m^2 (e.g., [37–39]). On the other hand, ERS dominated by emission from radio lobes show lower values of RMs, that is, from a few tens to hundreds of rad/m^2 (e.g., [40]).

3. Polarization Data on ERS at cm and mm Wavelengths

3.1. Polarization Surveys at 1.4 GHz. A large-scale polarization catalogue of radio sources is provided by the NRAO VLA Sky Survey (NVSS) at 1.4 GHz [41]. This survey covers $\Omega \simeq 10.3$ sr of the sky with $\delta \geq -40^\circ$. The catalogue contains the flux density S and the Stokes parameters Q and U of almost 2×10^6 discrete sources with $S \gtrsim 2.5$ mJy. Extensive analyses of these data were carried out by [20] and [16]. By correlating NVSS sources with sources from the Green Bank 4.85 GHz (GB6) catalogue [42], statistical polarization properties have been derived for a subsample of $\sim 30,000$ ERS with $S_{1.4\,\mathrm{GHz}} \geq 100$ mJy, divided into steep- and flat-spectrum sources. Steep-spectrum sources are found to increase the degree of polarization (Π) with decreasing flux density: in fact, the median (mean) Π value increases from $\Pi \simeq 1.1\%$ ($\simeq 2\%$) for $S > 800$ mJy up to $\Pi \simeq 1.8\%$ ($\simeq 2.7\%$) for the faintest ERS of the sample, at $100 \leq S < 200$ mJy. On the other hand, flat-spectrum sources show a lower fractional polarization (median $\sim$1.3% and mean $\simeq$ 2%) with no significant trend with flux density [16].

Two recent sub-mJy surveys at 1.4 GHz with polarization measurements, that is, the Dominion Radio Astrophysical Observatory (DRAO) *Planck* Deep Fields project [3, 23, 43] and the Australia Telescope Low-Brightness Survey (ATLBS) [22], seem to confirm the above result of a higher level of fractional polarization in steep-spectrum sources with fainter flux densities. However, there is no clear explanation for the origin of the anticorrelation between Π and flux density in this source population.

In Figure 1 we plot differential number counts at 1.4 GHz for the polarized intensity, computed from the surveys presented above. The continuous curve represents a fit to total number counts of AGNs from [44], whereas the dotted curve is obtained from the previous fit by assuming a constant fractional polarization of $\Pi = 3.3\%$ for *all* ERS.

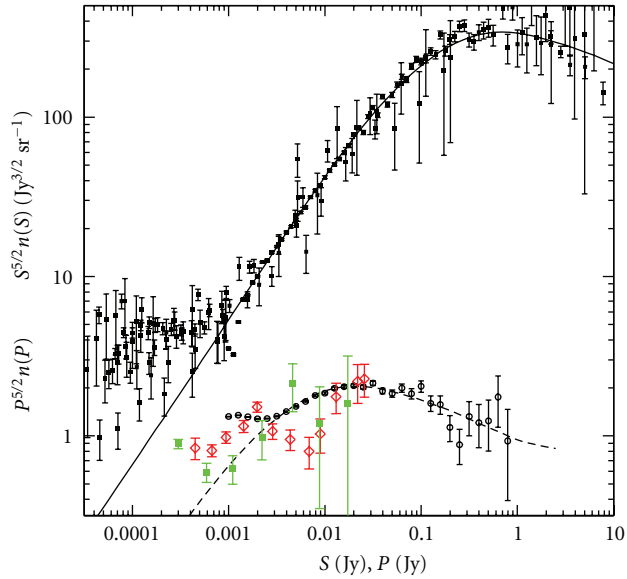

Figure 1: Differential number counts at 1.4 GHz as a function of total intensity (upper points) and of polarized intensity (lower points: black empty circles from NVSS; red empty diamonds from DRAO *Planck* Deep Fields; green squares from ATLBS). The continuous curve represents the number counts of AGNs from [44], whereas the dotted curve is obtained by the previous counts and assuming a constant fractional polarization of 3.3% for all ERS.

This value is chosen in order to fit NVSS data; the fit is extremely good down to polarized intensities of $P \simeq 3$ mJy. At fainter P fluxes the predicted curve bends down whereas observational data keep a flatter shape, in agreement with a higher fractional polarization for ERS at fainter flux density levels.

3.2. Multiwavelength Samples of Polarized ERS

3.2.1. Linear Polarization in a Sample of the B3-VLA Survey. Polarization measurements of sources in the B3-VLA survey [45] were carried out by [46] at 10.5, 4.85, and 2.7 GHz using the Effelsberg 100 m telescope. Taking into account only sources with $S_{10.5\,\mathrm{GHz}} \geq 80$ mJy, a sample of 106 objects (out of 208) was defined with detected polarization. They found that flat-spectrum sources are significantly less polarized than steep-spectrum ones at 10.5 GHz. The latter ERS population shows a median fractional polarization that strongly depends on the frequency, from $\sim$2% at 1.4 GHz to $\sim$6% at 10.5 GHz, indicating a high Faraday depolarization at lower frequencies. Moreover, they notice that compact steep-spectrum sources exhibit much stronger depolarization than noncompact ones, and that sources showing larger linear size are more polarized. On the other hand, flat-spectrum sources are characterized by almost constant and low degrees of polarization ($\sim$2.5%) over the whole wavelength range considered.

3.2.2. The Australia Telescope 20 GHz (AT20G) Survey. The AT20G survey is a blind survey of the whole Southern sky

at 20 GHz with follow-up observations at 4.8 and 8.6 GHz carried out with the Australia Telescope Compact Array (ATCA) [4]. The full source catalogue includes 5890 sources detected above a flux-density limit of 40 mJy. The AT20G catalogue is found to be 91% complete above 100 mJy and 79% above 50 mJy in regions south of declination -15°. Polarization was detected at 20 GHz for 768 sources, 467 of which also have simultaneous polarization detections at 5 and/or 8 GHz (upper limits on the polarized flux density are provided for nondetections, as described in [4]). Taking into account upper limits, a median (mean) fractional polarization of 2.6% (2.7%) at 20 GHz is found for sources with $S_{20\,\mathrm{GHz}} > 250$ mJy, whereas an average 17% depolarization is observed at 5 GHz with respect to 20 GHz [47]. Compact sources with detected polarization are separated into flat- and steep-spectrum sources: the mean values of Π are 2.9% and 3.8%, respectively, thus confirming the higher fractional polarization in steep-spectrum sources.

3.2.3. VLA Polarization Measurements of WMAP Point Sources. Using the VLA, [48] carried out polarization measurements at 8.4, 22 and 43 GHz of a complete sample of ERS brighter than 1 Jy in the 5-year WMAP catalogue and with declinations north of -34°. The sample consists of 203 objects: polarized emission was detected for 123, 169, and 167 sources at 8.4, 22, and 43 GHz, respectively, (at 8.4 GHz only a subset of 134 were observed) and 105 were detected at all the 3 frequencies. An accurate analysis of the statistical properties of the polarized intensity of the sample is done by [39], including an analysis of the correlations between the fractional polarization and the spectral indices. Here below, we summarize the main results obtained by them.

(i) The distribution of the fractional polarization varies slightly as a function of the frequency. Including sources undetected in polarization, the mean fractional polarization is $\langle\Pi\rangle = 2.9$ 3.0 and 3.5 percent at 8.4, 22, and 43 GHz.

(ii) No correlation is found between the fractional polarization at 22 GHz and the intensity spectral indices, α_8^{22} and α_{22}^{43} (we remind readers that the sample, selected at 22 GHz, is dominated by flat-spectrum sources).

(iii) There is a significant change in the polarization angle between 8.4 and 22 GHz. For 45 sources, the position angle satisfies the λ^2 dependence, and intrinsic rotation measures in excess of 1000 rad m^{-2} were observed for a large number of them.

(iv) Polarization of 71 sources was also measured at 86 GHz by [49]. The fractional polarization is typically higher at 86 GHz than at 43 GHz.

3.2.4. VLA Polarization Measurements in an ACT Survey Field. In [50], VLA observations in total intensity and polarization at 4.86, 8.46, 22.46, and 43.34 GHz are presented. The sample is selected from the AT20G survey and consists of 159 ERS, out of the almost 200 sources with flux density $S_{20\,\mathrm{GHz}} > 40$ mJy in a field of the Atacama Comsmology Telescope (ACT) survey. Polarized emission for about 60 sources was detected at all 4 frequencies, whereas the detections are 141, 146, 89, and 59 from low to high frequencies. Fractional polarization distributions are very similar at 5 and 8.5 GHz, whereas a trend of increasing polarization with increasing frequency is indicated at 22 and 43 GHz. In particular, a tail of strongly polarized ($\gtrsim 10\%$) sources is observed at 43 GHz. Data at 22 and 43 GHz suggest also that the polarization fraction in steep-spectrum sources is significant higher than in flat-spectrum sources.

3.3. Other Samples of Polarized ERS at High Frequencies

(i) Reference [51] presented polarization observations of 250 (out of 258) southern sources in the complete 5-GHz 1-Jy sample of [52] by using the ATCA facilities at 18.5 GHz. Polarized flux densities were measured for 170 sources (114 flat-spectrum and 56 steep-spectrum), upper limits were set for an additional subset of 27 sources (12 flat-spectrum and 15 steep-spectrum), and 53 sources were rejected (probably extended objects). The final flat-spectrum sample is almost complete (80%), while only 49% of steep-spectrum sources have reliable detections. In the flat-spectrum sample the median fractional polarization is $\simeq 2.7\%$ and the mean $\simeq 2.9\%$, and no sources have $\Pi > 10\%$. The median fractional polarization for the flat-spectrum sources included in the NVSS catalogue is about a factor 2 lower than that at 18.5 GHz. However, a relevant increase in the polarization fraction at 18.5 GHz is noticed only for sources with $\Pi \lesssim 1\%$ at 1.4 GHz.

(ii) Reference [49] presented a 3.5 mm polarimetric survey of ERS using the IRAM 30 m Telescope. Their sample consists of 145 flat-spectrum sources with $\delta > -30^\circ$ and flux density $\gtrsim 1$ Jy at 86 GHz. Linear polarization is detected for 76% of the sample (110 objects). They found that BL Lacs ($\Pi_{\mathrm{median}} \simeq 4.4\%$) are more strongly polarized than quasars ($\Pi_{\mathrm{median}} \simeq 3.1\%$). This result seems to be in contradiction with the idea that quasars should be more polarized at high frequencies than BL Lacs because in the latter sources the synchrotron self-absorbed spectrum is maintained up to higher frequencies. A possible explanation provided by the authors comes from the recent evidence that the view angle of jets in quasars is smaller than that in BL Lacs [53, 54]. So, if the magnetic field is not homogeneous along the jet, a lower fractional polarization level is expected from sources better oriented to the line of sight (i.e., quasars).

Moreover, for those sources with detected polarization at 15 GHz, they found that $\Pi_{86\,\mathrm{GHz}}$ is larger than $\Pi_{15\,\mathrm{GHz}}$ by a median factor ≈ 2, and about 20% of sources have the $\Pi_{86\,\mathrm{GHz}}/\Pi_{15\,\mathrm{GHz}}$ ratio larger than 4. Reference [49] suggest that this increase may be explained by a combination of two phenomena: the 86-GHz emission comes from a region with

Table 1: Median, mean, and $\langle \Pi^2 \rangle^{1/2}$ of the fractional polarization for flat-spectrum sources in the almost complete subsample of the AT20G surveys at different observational frequencies and flux ranges. $N_{\rm tot}$ refers to the total number of objects in the corresponding flux range; $N_{\rm multi}$ to the number of objects with 5- and 8-GHz measurements; $N_{\rm fl}$ to the number of flat-spectrum sources; $N_{\rm det}$ to the number of flat-spectrum sources with polarization detection.

S(Jy)	$N_{\rm tot}$	$N_{\rm multi}$	$N_{\rm fl}$	$N_{\rm det}$	$\Pi_{\rm med}$	$\langle \Pi \rangle$	$\langle \Pi^2 \rangle^{1/2}$
				20 GHz			
≥1.0	130	114	110	85	2.05	2.82	3.72
≥0.5	315	287	264	188	2.01	2.76	3.84
[0.5, 1)	185	173	154	103	1.92	2.72	3.92
				8.6 GHz			
≥1.0			110	87	2.00	2.52	3.00
≥0.5			264	180	1.76	2.34	2.85
[0.5, 1)			154	93	1.54	2.21	2.73
				4.8 GHz			
≥1.0			110	93	1.90	2.31	2.71
≥0.5			264	186	1.71	2.25	2.69
[0.5, 1)			154	93	1.59	2.20	2.68

greater degree of order in the magnetic field or/and, at 15 GHz, emission is still affected by Faraday depolarization.

(iii) Reference [55] looked for polarized sources in the *WMAP* five-year data, using a new technique named *filtered fusion*. They detected polarization in 13 ERS at a confidence level ≥ 99% and polarized flux density higher than 300 mJy.

4. Statistical Properties of the Polarized Emission in ERS

In order to provide reliable estimates of ERS contamination to CMB anisotropy polarization measurements, we need to address the following main questions about polarization properties of ERS: (1) how the fractional polarization, Π, varies from cm to mm wavelengths; (2) *if* the fractional polarization depends on the flux density; (3) how polarization properties change among the different populations of ERS. In this section we address these questions on the basis of the observational data presented and discussed in the previous Section.

4.1. Flat-Spectrum Sources. We investigate more deeply the polarization of ERS observed in the AT20G survey. We consider the almost-complete sample at $\delta < -15^\circ$ and, when available, we use 5- and 8-GHz measurements to separate ERS into steep- and flat-spectrum sources. In Table 1 we report statistical properties of the fractional polarization (i.e., the mean $\langle \Pi \rangle$, the median $\Pi_{\rm med}$, and $\langle \Pi^2 \rangle^{1/2}$) for flat-spectrum sources as a function of the flux density range and the frequency. They are computed using the Survival Analysis techniques and the Kaplan-Meyer estimator as implemented in the ASURV code [56], which takes into account upper limits on the fractional polarization for estimating the above quoted quantities. In fact, when polarization is not detected, an upper limit is provided. About 10% of sources in the AT20G sample we use here have measurements only at 20 GHz (see Table 1). Although most of them should be flat-spectrum sources, for a more consistent comparison with results at 5 and 8 GHz we prefer to exclude them from the analysis.

At 20 GHz the median and the mean fractional polarization do not present any significant variation between the subsamples defined by $S \geq 1$ Jy and $0.5 \leq S < 1$ Jy. At the lower frequencies, $\langle \Pi \rangle$ and $\Pi_{\rm med}$ show a moderate decrease at fainter flux densities. In particular, two-sample tests implemented in the ASURV code (e.g., the Gehan's generalized Wilcoxon test and the Peto & Prentice generalized Wilcoxon test) yield a probability of ∼10% and ∼1% that the distributions of the fractional polarization for $S \geq 1$ Jy and $0.5 \leq S < 1$ Jy at 5 and 8 GHz, respectively are drawn from the same parent distribution (compared to a probability of 30% at 20 GHz). At flux densities lower than 500 mJy, the high number of upper limits ($\gtrsim$ 50%) makes our estimates unreliable.

On the other hand, a larger fractional polarization is observed as the frequency increases, with, on average, ≈18% of depolarization at 5 GHz with respect to 20 GHz, in agreement with results from [47]. The ASURV two-sample tests yield only a 10% probability to have the same parent distribution for Π at 5 and 20 GHz. For a better comparison, we show in Figure 2 the distributions of the fractional polarization discussed above as obtained by using the Kaplan-Meyer estimator. These distributions are well fitted by a log-normal distribution with $\Pi_{\rm med}$ and $\langle \Pi^2 \rangle$ values taken from Table 1 (see, e.g., the case at 20 GHz in Figure 2). (Figure 2 clearly shows that the log-normal distribution, when averaged in each Π bin, is giving predictions always compatible with the observed Π values well inside the 1σ level, except for very few bins at high Π levels where the statistics is very poor. We have also verified

that adopting other distribution functions, for example, a truncated gaussian, we are not able to reproduce equally well the observed distributions of Π.)

In Figure 3 we also study the correlation of $\Pi_{20\,\mathrm{GHz}}$ with $\Pi_{4.8\,\mathrm{GHz}}$ and $S_{20\,\mathrm{GHz}}$: no clear correlation is found between the fractional polarization and the flux density at 20 GHz (the generalized Kendall's tau test yields a probability $P \sim 60\%$ of no correlation). On the other hand, as expected, we see a strong correlation between the fractional polarization at 20 and 4.8 GHz (with a $P < 0.01\%$ of no correlation). Using the Schmitt's method from the ASURV code, we find a linear regression $\Pi_{20\,\mathrm{GHz}} = 1.58 + 0.46\Pi_{4.8\,\mathrm{GHz}}$. This result seems to indicate that only sources with very low fractional polarization at 5 GHz (i.e., $\Pi_{4.8\,\mathrm{GHz}} \lesssim 2\%$) have a significant increase of Π at 20 GHz (see also Figure 3). The large offset term in the linear regression we find, however, could be also partially due to Eddington bias in the AT20G catalogue and to the large number of sources with upper limits in fractional polarization at $\Pi \gtrsim 1\%$.

In Figure 5 we plot the mean and median values of the fractional polarization as obtained from the surveys presented in the previous section. These data allow us to cover frequencies from 1.4 to 86 GHz. Although there is large scatter in the data, we see a general increasing trend for the median fractional polarization: Π_{med} is ∼1.5% at 1.4 GHz, around 2–2.5% in the range 5–10 GHz, and finally 2-3% at $\nu > 10$ GHz. The mean fractional polarization has a more linear increase with the frequency in all the samples, with $\langle\Pi\rangle$ varying from 2–2.5% at 1.4 GHz to 3–3.5% at $\nu \geq 20$ GHz.

Most of the data presented in Figure 5 are coming from samples of bright sources, typically with $S \gtrsim 1$ Jy. Samples with fainter sources are the B3-VLA ($S_c = 80$ mJy) and the sample discussed in [50]. The latter one provides polarization for sources with $S \geq 40$ mJy. However, since at the frequencies 20 and 43 GHz the number of polarized ERS detected in the sample is less than 50 percent, we have decided to consider only flat-spectrum sources with $S \geq 80$ mJy. Spectral indices are estimated using flux densities at 4.86 and 8.46 GHz. Table 2 reports the number of detections and the corresponding values of the mean, median, and $\langle\Pi^2\rangle^{1/2}$ of the fractional polarization. For the two highest frequencies of the sample we estimate the median in two ways: firstly, we use the ASURV code, by taking into account the upper limits; secondly, we assume a fractional polarization ≤1% for those sources without measured polarization (values indicated in brackets in Table 2). The large spread between the two values at 43 GHz is an indication that the sample, also including upper limits, could provide biased values of statistical properties of Π at these frequencies.

If we compare results from the previous two samples (i.e., B3-VLA and [50]) with surveys of bright sources, we cannot find any clear evidence of higher fractional polarization in faint sources. However, larger and deeper samples of data are clearly required to settle the question.

In Figure 5 we also include the $\langle\Pi^2\rangle^{1/2}$ values. This quantity is important in order to estimate the angular power spectra of the polarized signal due to undetected ERS. At $\nu > 20$ GHz, that is, the most interesting frequencies for CMB data analyses, sources have $\langle\Pi^2\rangle^{1/2} \sim 4\%$. In [49] optical identifications are provided for ERS in the [50] sample. Over a total of 145 objects, 107 are identified as quasars and 26 as BL Lacs: we find $\Pi_{\mathrm{med}} = 3.0\%$, 3.6% and $\langle\Pi^2\rangle^{1/2} = 3.8\%$, 4.5% for FSRQs and BL Lacs, respectively.

4.2. Steep-Spectrum Sources. The number of steep-spectrum sources with polarization measurements becomes very small at frequencies $\gtrsim$ 10 GHz, preventing any study of the correlation between fractional polarization and flux density (see, e.g., Figure 4). In the subsample of AT20G at $\delta < -15^\circ$ there are 51 steep-spectrum sources with $S \geq 0.3$ Jy and only 25 of them have polarization detected at 20 GHz. We find that the median fractional polarization for these sources is less than 2% at all the frequencies (see Figure 5(b)). These very small values could be biased due to the small number of detected sources and to the incompleteness of the sample at faint flux densities. Nevertheless, from Figure 4 we can see a general increase of the fractional polarization between 4.8 and 20 GHz: the ratio of Π at 20 and 4.8 GHz is typically close to one (<1.5) for sources with $\Pi_{4.8\,\mathrm{GHz}} > 2\%$, but become higher for sources weakly polarized at 4.8 GHz. In fact, the linear regression found by the Schmitt's method implemented in the ASURV code yields $\Pi_{20\,\mathrm{GHz}} = 0.78 + 1.14\,\Pi_{4.8\,\mathrm{GHz}}$.

From Figure 5 we can observe the strong increase of the fractional polarization from 1.4 GHz to 5 GHz, where Faraday depolarization is probably very relevant. The increase becomes more moderate up to 20 GHz. The large difference in the median values among different samples is perhaps related to the small samples considered and the large fraction of sources with upper limits in polarization. The largest sample of steep-spectrum sources is provided by B3-VLA (77 sources, all with detected polarization) and the Ricci et al. sample (71 sources, 15 of them with upper limits): in these samples the median fractional polarization is ∼5% between 5–20 GHz and the mean varies from 5 to 6.5%.

4.3. Number Counts in Polarization of ERS at 20 GHz. We provide a first estimate of number counts in polarization, $n(P)$, at 20 GHz by exploiting WMAP and AT20G polarization source catalogues. For very bright sources, we use the polarized source sample detected by [55] in the 5 yr WMAP CMB anisotropy maps (see their Table 2). We exclude from number counts Fornax A, Virgo A, and Centaurus A because they are all local objects. Then, we consider the nearly-complete subsample of AT20G at $\delta < -15^\circ$ and $S \geq 50$ mJy. This sample allows us to compute $n(P)$ down to polarized fluxes of ∼10 mJy. Number counts, that are reported in Table 3 (see also Figure 6), have been corrected for the estimated incompleteness of the sample (i.e., the completeness is 0.91 for $S \geq 100$ mJy and 0.79 for $50 \leq S < 100$ mJy [4]). As displayed by Figure 6, number counts in total polarization, $n(P)$, are almost flat at 20 GHz, at least in the flux density range in which they can be estimated.

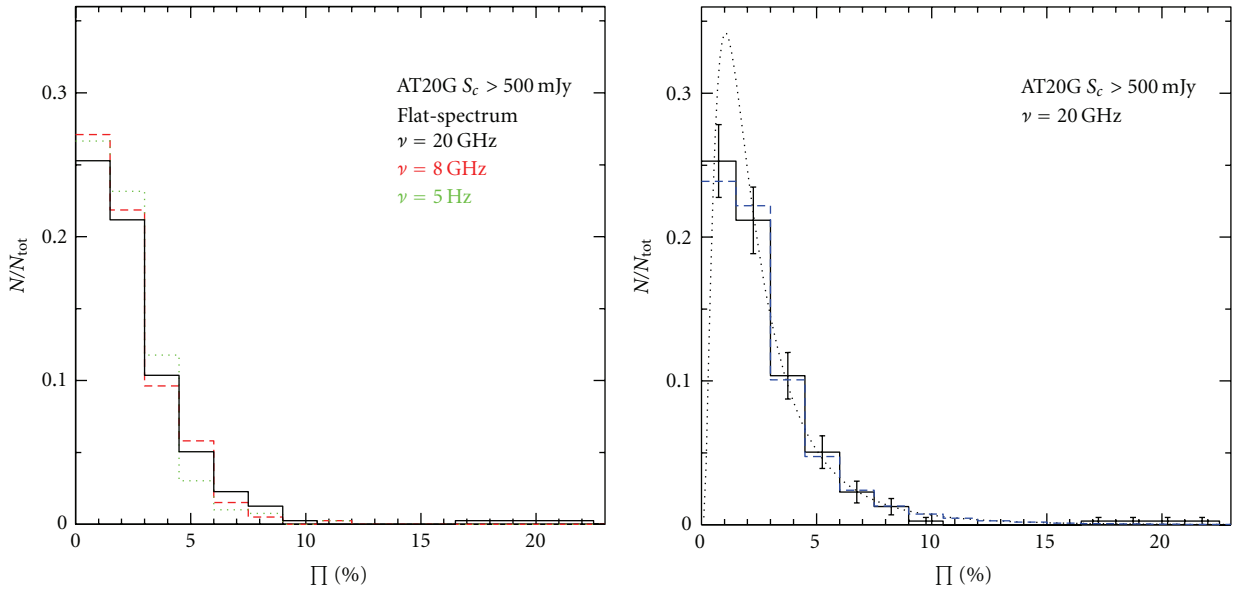

(a) (b)

Figure 2: (a) Distribution of the fractional polarization at 4.8, 8.6, and 20 GHz (green dotted, red dashed, and black solid histograms, resp.) for flat-spectrum sources with $S \geq 500$ mJy in the almost-complete subsample of the AT20G survey. (b) Distribution of the fractional polarization at 20 GHz (black solid histogram) compared to the distribution (blue dashed histogram) produced by a log-normal distribution (see also Section 5.1) with $\Pi_{med} = 2.01$ and $\langle \Pi^2 \rangle = 3.84$ (black dotted line; see Table 2) at 20 GHz.

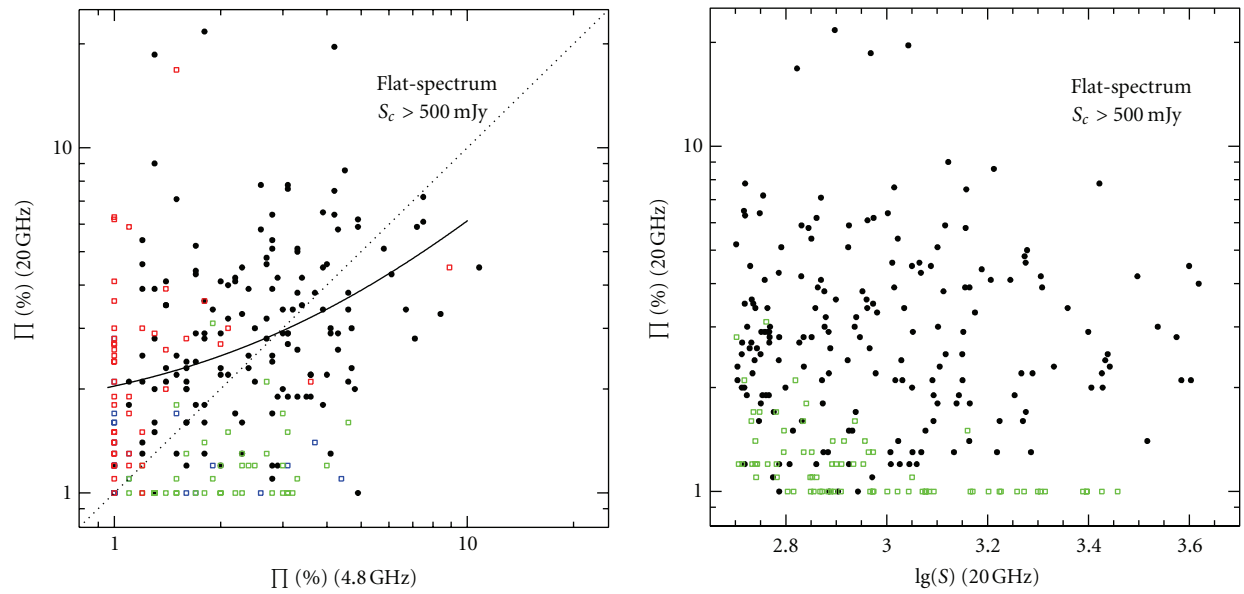

(a) (b)

Figure 3: (a) Correlation between fractional polarizations at 4.8 and 20 GHz for flat-spectrum sources with $S \geq 500$ mJy. Green points indicate upper limits in Π at 20 GHz, red points at 4.8 GHz, and blue points at the both frequencies. The solid line is the linear regressions found by the ASURV code (see the text). (b) The fractional polarization at 20 GHz as a function of the flux density at the same frequency (green points indicate upper limits in Π).

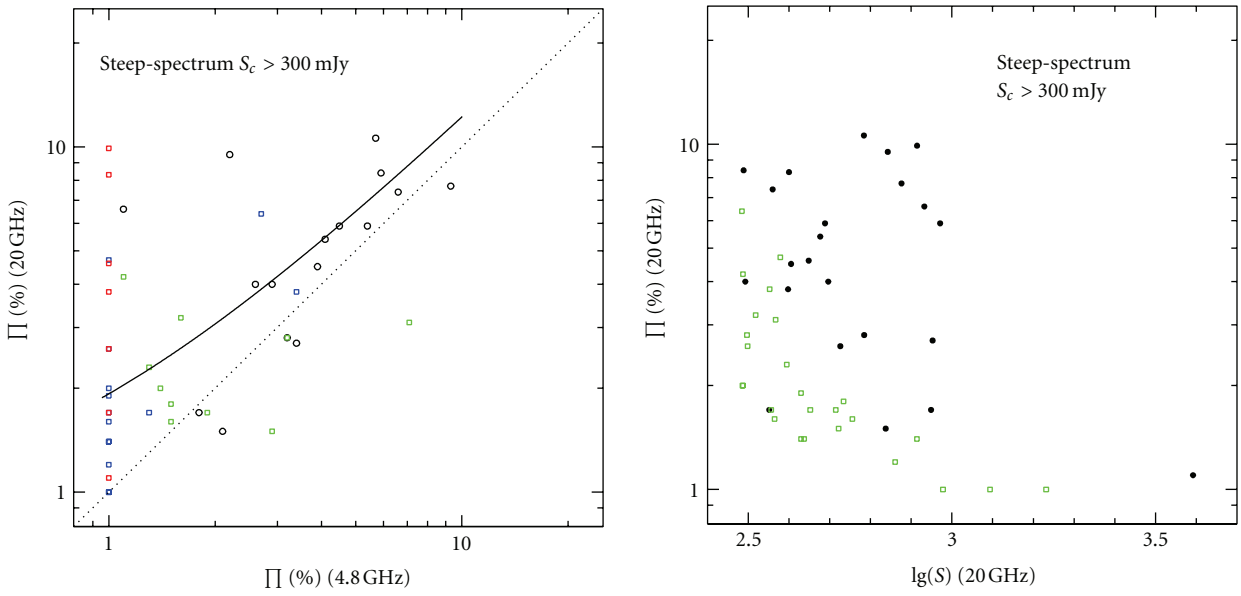

Figure 4: Fractional polarization for steep-spectrum sources at 20 GHz as a function of fractional polarization at 4.8 GHz (a) and of flux density at 20 GHz (b). Points of different colours have the same meaning as in Figure 3.

Table 2: Median and mean of the fractional polarization and $\langle \Pi^2 \rangle^{1/2}$ from the Sajina et al. [50] sample. For flat-spectrum sources we consider only objects with $S \geq 80$ mJy. Median values in brackets are computed by assigning a value of $\Pi < 1\%$ to sources without a detection in polarization.

Flat-spectrum sources						
ν[GHz]	N_{sou}	N_{det}	Π_{med}		$\langle \Pi \rangle$	$\langle \Pi^2 \rangle^{1/2}$
4.86	56	54	2.16		2.47	2.97
8.46	56	55	2.25		2.61	3.10
22.46	56	44	3.12	(2.88)	3.79	4.21
43.34	50	33	4.14	(2.64)	4.85	5.79
Steep-spectrum sources						
4.86	45	44	2.56		4.10	5.79
8.46	45	44	3.48		4.67	5.97
22.46	44	25	6.14	(3.40)	7.17	8.03
43.34	28	11	6.77		7.18	8.30

Given that an upper limit on the fractional polarization Π_{up} is always provided for the ERS in this sample (see [4], for more details), except for 5 very bright objects with no information on polarization, we also give a tentative estimate (Table 3, third column) of their contribution to the number counts $n_i^{up}(P)$ between P_i and $P_i + \Delta P$ by means of

$$n_i^{up}(P) = \sum_k \int_{\Pi_i}^{\Pi_f} \mathcal{P}(\Pi) d\Pi \quad \text{with } \Pi_i = \frac{P_i}{S_k},\ \Pi_f = \frac{P_i + \Delta P}{S_k}. \tag{1}$$

The sum is done over all the sources without polarization detection and S_k is the flux density of the kth object. $\mathcal{P}(\Pi)$ is the probability function for the fractional polarization: we take a log-normal function with $\Pi_{med} = 2.0\%$ and $\langle \Pi^2 \rangle^{1/2} = 2.8\%$ (see Table 1 and Figure 3) if $\Pi \leq \Pi_{up}$ and zero otherwise. For the 5 objects without any polarization information, no upper limits are considered.

As shown by Table 3 and Figure 6, the contribution of sources undetected in polarization (displayed by empty squares) is generally negligible, except for bins at very faint polarization levels (i.e., less than 20 mJy), and for bins at $P \gtrsim 100$ mJy, due to the 5 sources without polarization information and flux density between 1 and 10 Jy. Only for the faintest bin n_i^{up} is larger than the uncertainty on the number counts. Therefore, we can conclude that number

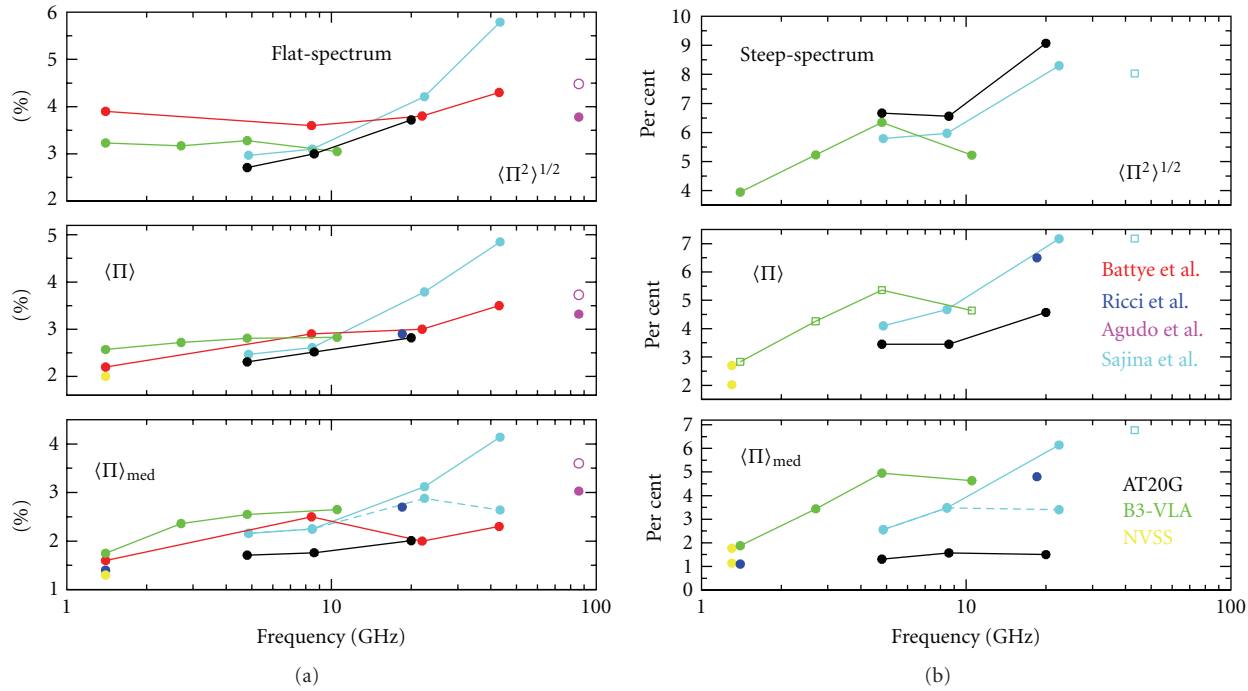

(a) (b)

FIGURE 5: Median, mean, and $\langle\Pi^2\rangle^{1/2}$ of fractional polarization for flat- (a) and steep-spectrum (b) sources. *Black points* refer to the almost complete subsample of the AT20G survey with $S_c = 500$ mJy for flat-spectrum sources and 300 mJy for steep-spectrum sources. *Red points* refer to data presented in [39]. *Green points* refer to the B3-VLA sample (with respect to [46], we distinguish flat- and steep-sources on the basis of their spectral index between 1.4 and 5 GHz; values shown in the plot are obtained using the ASURV code, taking into account upper limits in the fractional polarization). *Cyan points* refer to the sample from [50] (see text and Table 2; empty cyan points at 43 GHz for the steep-spectrum have to be considered as upper limits). *Blue points* refer to results from [51] and *magenta points* from [49] (solid and empty points are for FSRQs and BL Lacs, resp.). *Yellow points* refer to the NVSS survey (see [16]): for steep-spectrum sources we plot results for sources with $100 \leq S < 200$ mJy and $S \geq 800$ mJy.

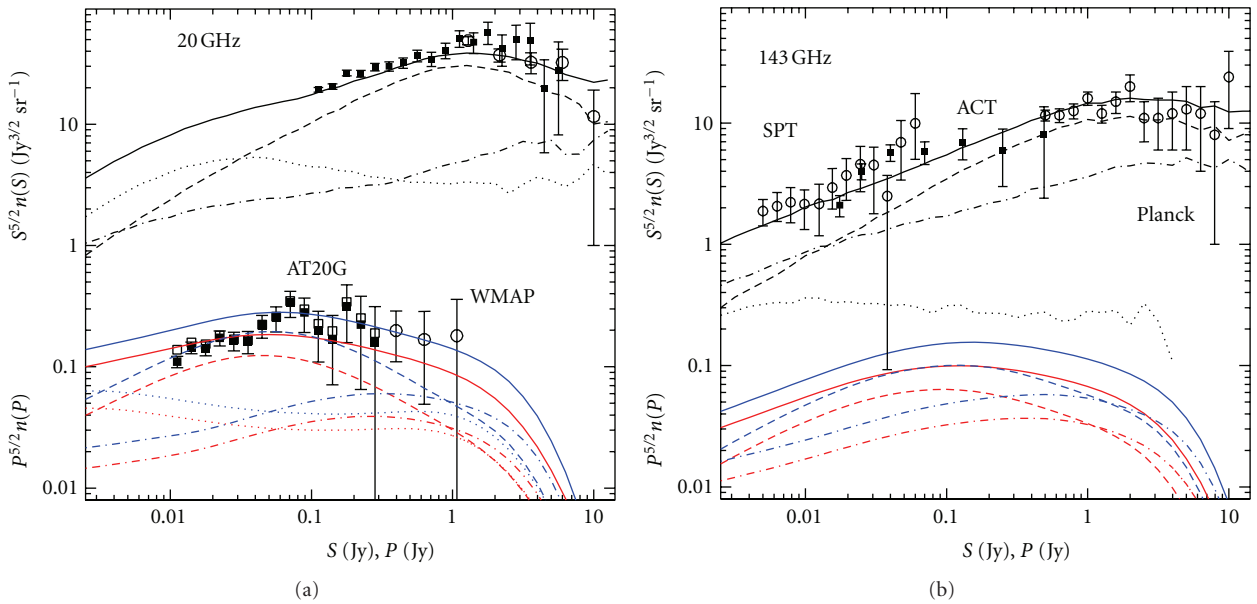

(a) (b)

FIGURE 6: Normalized number counts at 20 (a) and at 143 GHz (b) in total intensity (upper curves and data points) and in polarized intensity (lower curves and data points; blue curves are for the more "conservative" case and red curves for the more "optimistic" case). Number counts are for the different source populations discussed in the text: solid lines represent total number counts; dotted lines are for steep-spectrum sources; long-dashed lines are for FSRQs; finally, dot-dashed lines are for BL Lacs. In (a), filled squares represent our current estimates from the AT20G subsample (empty squares include the contribution from sources without polarization detection; see Section 4.3) and empty circles are from WMAP 5-years data [55]. Data points in (b) are from published data [57–59].

counts in polarization estimated from the AT20G sample are not affected by upper limits in the polarized flux density.

5. Cosmological Evolution Models and High-Frequency Number Counts of ERS

Early evolutionary models of radio sources [17, 60–62] were able to give remarkably successful fits to the majority of data coming from surveys at $\nu \lesssim 10$ GHz, and down to flux densities of a few mJy. More recently, [18, 44] exploited the wealth of newly available data on luminosity functions, multifrequency source counts and redshift distributions to provide new cosmological evolution models of radio sources at frequencies $\gtrsim 5$ GHz and $\lesssim 5$ GHz, respectively. These two models are based on the determination of the epoch-dependent luminosity functions for different source populations, starting from the local luminosity function and by adopting different luminosity evolution laws with free parameters fitted from observational data.

The predictions of high-frequency number counts of ERS provided by the above evolution models assume a simple power-law spectrum for ERS. Each source population is characterized by an "average," fixed, spectral index, or by two spectral indices (at most). This "classical" modeling has to be considered as a first-although successful-approximation, but it gives rise to an increasing mismatch with observed high-frequency (>30 GHz) number counts currently available.

Indeed, the ERS energy spectra can be quite different from a single power-law if analyzed in large frequency intervals. Different mechanisms can be responsible for this: (a) a spectral steepening due to the more rapid energy loss of high-energy electrons with source age, that is, "electron ageing"; (b) a transition from the optically thick to the optically thin regime at high radio frequencies; (c) at different wavelengths radio emission can be dominated by different components characterized by distinct spectral behaviors [63]. In particular, a clear steepening at mm wavelengths is theoretically expected for radio flat spectra of AGN core emission [64, 65]. This steepening has been already observed in blazars (see, e.g., [66]) and has also been statistically suggested by recent analyses of different ERS samples at $\nu > 30$ GHz [19, 59, 67–69].

A first attempt of taking such steepening in blazar spectra into account has been done by [19]. In this work the spectral behaviour of blazars at mm wavelengths is statistically described by considering the main physical mechanisms responsible for the emission. In agreement with classical models of the synchrotron emission in the inner jets of blazars these authors interpret the high-frequency steepening observed in blazar spectra as caused, at least partially, by the transition from the optically-thick to the optically-thin regime in the observed spectra at mm wavelengths. Based on the published models of synchrotron emission from inhomogeneous, unresolved, relativistic jets [30, 65, 70], the value of the frequency ν_M at which the spectral break occurs is estimated as a function of the relevant physical parameters of AGNs: the redshift, the Doppler factor, and the linear dimension of the region (approximated as homogeneous and spherical) that is mainly responsible for the emission at the break frequency.

Recent high frequency data [57, 58], and in particular the first 1.6 *Planck* survey [59], have provided new important results on number counts and related statistics of ERS, and they can be used to constrain the different possible cases/models featuring a spectral break in the emission of AGN jets (see [19]). The most successful one (indicated in [19] as C2Ex, that is, the relevant emission is emitted from a more "extended" region in the inner jet of FSRQs) assumes different distributions of the break frequency for BL Lacs and FSRQs. According to this model, most of the FSRQs should show a bend in their otherwise flat spectra between 10 and 100 GHz, whereas in BL Lac spectral breaks should be typically observed at $\nu > 100$ GHz (implying that the observed synchrotron radiation comes from more compact emitting regions). This dichotomy has been indeed found in the *Planck* ERCSC [66, 71]: almost all radio sources show very flat spectral indices at LFI frequencies, $\alpha_{\mathrm{LFI}} \gtrsim -0.2$; at HFI frequencies BL Lacs keep flat spectra ($\alpha_{\mathrm{HFI}} \gtrsim -0.5$) while most of FSRQs show steeper spectra, that is, $\alpha_{\mathrm{HFI}} < -0.5$. Moreover, the same model gives a remarkably good fit to all the observed data on number counts and spectral index distributions of ERS at frequencies above 5 and up to 220 GHz.

For the above reasons, hereafter we adopt the number counts provided by the "C2Ex" case in [19].

5.1. Number Counts of ERS in Polarization at mm Wavelengths. To assess the contamination due to undetected ERS in CMB polarization maps it is necessary to know how many sources can be found with polarized flux density $P = \sqrt{\mathrm{Q}^2 + U^2}$ (typically, a debiased estimator is however used for the polarized flux density of point sources (as, for example, $P = \sqrt{Q^2 + U^2 - s^2}$, where s is the uncertainty on P; see [50] for more details)) above a given flux limit P_{lim}. Answering this question involves the determination of source counts in polarization. This estimate is quite difficult to perform directly, by the statistical analysis of observational data, since the polarized signal is weak and many samples are usually defined by their completeness in terms only of total intensity. However, this problem can be overcome by using the source number counts in total intensity complemented by information on the statistical properties of the fractional polarization Π, expressed in term of some probability function $\mathcal{P}(\Pi)$ [16].

Let us discuss this point in more detail. Polarization number counts $n(P)$ can be written as

$$n(P) = N \int_{S_0=P}^{\infty} \mathcal{P}(P, S) dS = N \int_{S_0=P}^{\infty} \mathcal{P}(\Pi, S) \frac{dS}{S}, \quad (2)$$

where N is the total number of sources with $\mathrm{S} \geq S_0$ in the sample, $\mathcal{P}(P, S)$ and $\mathcal{P}(\Pi, S)$ are the probability functions of observing in a source of flux density S, a polarized intensity P and a fractional polarization Π, respectively. Assuming that Π is independent of S, $n(P)$ can be determined by

$$n(P) = \int_{S_0=P}^{\infty} \mathcal{P}\left(\Pi = \frac{P}{S}\right) n(S) \frac{dS}{S}. \quad (3)$$

Table 3: Number counts in polarization at 20 GHz from WMAP and AT20G source catalogues. $N_{\rm det}$ indicates the number of objects with detected polarization, while $n^{\rm up}(P)$ is the estimated contribution of AT20G objects with no polarization information or with upper limits in the fractional polarization.

		AT20G subsample		
P (mJy)	$N_{\rm det}$	$n(P)$	$\sigma_{n(P)}$	$n^{\rm up}(P)$
11.2	87	$0.828E+04$	$0.889E+03$	$0.205E+04$
14.1	81	$0.607E+04$	$0.675E+03$	$0.636E+03$
17.8	57	$0.338E+04$	$0.447E+03$	$0.263E+03$
22.4	49	$0.231E+04$	$0.329E+03$	$0.102E+03$
28.2	33	$0.123E+04$	$0.215E+03$	$0.242E+02$
35.5	23	$0.683E+03$	$0.142E+03$	$0.112E+02$
44.7	22	$0.519E+03$	$0.111E+03$	$0.104E+02$
56.2	18	$0.337E+03$	$0.795E+02$	$0.938E+01$
70.8	17	$0.253E+03$	$0.613E+02$	$0.842E+01$
89.1	10	$0.118E+03$	$0.374E+02$	$0.752E+01$
112.2	5	$0.469E+02$	$0.210E+02$	$0.664E+01$
141.3	3	$0.224E+02$	$0.129E+02$	$0.385E+01$
177.8	4	$0.237E+02$	$0.118E+02$	$0.184E+01$
223.9	2	$0.941E+01$	$0.665E+01$	$0.121E+01$
281.8	1	$0.374E+01$	$0.370E+01$	$0.755E+00$
		5 yr WMAP sample		
398.1	5	$0.199E+01$	$0.889E+00$	
631.0	2	$0.530E+00$	$0.375E+00$	
1072.	1	$0.150E+00$	$0.150E+00$	

The probability function $\mathcal{P}(\Pi)$ can be constrained from the observed distributions of the fractional polarization. In agreement with [39] we model $\mathcal{P}(\Pi)$ by a log-normal distribution:

$$\mathcal{P}(\Pi) = \frac{1}{\sqrt{2\pi\sigma^2}\Pi} \exp\left\{-\frac{\left[\log(\Pi/\Pi_{\rm med})\right]^2}{2\sigma^2}\right\}, \qquad (4)$$

where $\Pi_{\rm med}$ is the median of the distribution and $\sigma^2 = 1/2\log(\langle\Pi^2\rangle/\Pi^2_{\rm med})$. These formulas are strictly valid only if $0 \leq \Pi < \infty$. However, because of the very low fractional polarization observed in ERS, the upper limit of $\Pi = 0.75$ can be effectively assumed as infinite. In Figure 2 we compared log-normal functions with the polarization distributions observed in the AT20G survey, confirming the very good fit of the model with data.

A critical point for our estimates is the variation with frequency of the fractional polarization observed in ERS. The data on ERS polarization discussed in this paper clearly show an higher fractional polarization at 10–20 GHz than at few GHz in both flat- and, more prominently, in steep-spectrum sources. At higher frequencies, data become scarce, but there are still indication of a possible further increase of the polarization fraction from 10–20 GHz to 40–90 GHz [39, 49]. For flat-spectrum sources, this increase could be due to the combination of two different effects: (1) the polarization degree actually increases with the frequency; and (2) BL Lacs, which are observed to be more polarized than quasars [49], become more relevant in number at higher frequencies.

In the following predictions we take into account both effects. We consider two possible values for the median and the dispersion $\langle\Pi^2\rangle^{1/2}$ of the log-normal distribution in order to provide a range of estimates for number counts and power spectra that could take into account uncertainties in observational data at $\nu > 10$ GHz. Table 4 reports our estimates for a more "optimistic" (lower) and a more "conservative" (upper) case. (Please note that the choice of the two adjectives, "optimistic" and "conservative", has been done under the point of view that polarized ERS do "contaminate" CMB maps in polarization and, thus, have to be removed from them.) The frequency dependence of the fractional polarization in ERS is simply modeled by means of two different sets of median and r.m.s. values at frequencies below and above about 40 GHz. Although somewhat arbitrary, this choice is motivated by the fact that this is the highest frequency at which multifrequency polarization samples of ERS are available.

(i) At $\nu \lesssim 40$ GHz we choose a lower and higher median and r.m.s. values of the fractional polarization based on the results displayed in Figure 5. Moreover, we require that number counts computed using values in Table 4 are (at least partially) compatible with AT20G/WMAP counts in polarization. As shown in Figure 6, the more "optimistic" case fits quite well with observational counts, especially at $P \lesssim 50$ mJy. On the other hand, the more "conservative" case tends to overestimate number counts at lower polarized fluxes, whereas it fits particularly well with

Table 4: Median and dispersion of the log-normal distribution for the fractional polarization, Π, as a function of frequency and for the different radio source populations relevant at CMB frequencies. Two cases are considered, a more "optimistic" one and a more "conservative" one (see Section 5.1).

	$\nu \lesssim 40$ GHz			$\nu > 40$ GHz		
	Steep	FSRQ	BL Lac	Steep	FSRQ	BL Lac
	Lower case (more "optimistic")					
$\Pi_{\rm med}$ (%)	3.0	2.0	2.5	4.0	2.5	3.0
$\langle\Pi^2\rangle^{1/2}$ (%)	5.0	3.0	3.5	6.0	3.5	4.2
	Upper case (more "conservative")					
$\Pi_{\rm med}$ (%)	4.0	3.0	3.6	5.0	3.6	4.3
$\langle\Pi^2\rangle^{1/2}$ (%)	6.0	3.8	4.5	7.0	4.6	5.5

current data at high P fluxes. This is not unexpected because, in this latter case, we take as median and dispersion of the fractional polarization for blazars the values provided by [49] at 90 GHz.

(ii) At $\nu > 40$ GHz, we make the assumption of an increase of the median fractional polarization of about 20% with respect to the corresponding cases at $\nu \lesssim 40$ GHz. This choice is not firmly constrained by current data sets; however, we have been guided by the fractional polarization levels of ERS observed by [49] at 86 GHz which fall in the middle between our present lower and upper cases.

In Figure 6 we compare the predicted number counts, $n(P)$, of ERS in polarized intensity at 20 and 143 GHz. By comparing the two panels of the same Figure we can appreciate that $n(P)$ decreases by a factor $\simeq 1.5$ at 143 GHz at $P \sim 0.1$ Jy, in comparison with the estimated $n(P)$ at 20 GHz. At still fainter polarized intensities, $P \sim 0.01$ Jy, this decrement increases due to the fact that the contribution of steep-spectrum ERS, which are on average more polarized, becomes less and less relevant at high CMB frequencies. Finally, Figure 6(b) indicates a possible higher relative contribution to total polarized counts, $n(P)$, coming from BL Lacs with respect to FSRQs at 143 GHz. This is a direct consequence of the present analysis, which is based on the observations discussed by [49].

The good agreement with observational data at 20 GHz, as well as the reliability of our predictions on ERS number counts in flux density, S, gives us confidence in making extrapolations of integral number counts, $N(>P)$, in total linear polarization at *Planck* frequencies (see Table 5). It is expected that *Planck* LFI will be able to detect sources in polarization down to $\simeq$ 200 mJy at 30 GHz and $\simeq$300–400 mJy at 44 and 70 GHz, whereas *Planck* HFI, thanks to a better resolution and sensitivity, should reach polarized flux limits of $P \approx 100$ mJy. In both cases, however, a catalogue of only a few tens of compact ERS should be provided by *Planck* in polarization.

The above quoted detection limits in total polarization are estimated by the performances foreseen for the *Planck* LFI and HFI instruments and are based on prelaunch measurements [12, 13] of the detectors calibration and capabilities. These detection limits take also into account the future application to the *Planck* data—corresponding to the end of the nominal mission, that is, in January 2012—of new detection techniques, specifically designed for detecting compact polarized sources in CMB maps (see, e.g., [72] for a recent discussion on the subject). These techniques have already been applied with success to WMAP 5 yr maps [55], improving on the results published by the WMAP team on the same data set.

6. Predictions on the Contribution of ERS to the CMB E- and B-Modes

As for temperature fluctuations, the analysis of CMB polarization measurements is usually made by the estimate of angular power spectra, that is, E- and B-modes spectra [8, 9]. B-mode polarization, that arises only from tensor perturbations, is expected to be extremely weak, and even for the most optimistic cases foreseen by inflationary models the rms signal is only a fraction of μK, less than 1 per cent of the level of temperature anisotropies at degree scales. On the other hand, polarization of foregrounds (and in particular of extragalactic sources) is equally shared between E- and B-modes [73]. ERS are therefore expected to dominate the sky B-mode polarization at subdegree angular scales at frequencies $\nu \lesssim 100$ GHz [74].

By using the statistical characterization of the fractional polarization described in the previous Sections, we are able to estimate the polarized angular power spectra given by undetected ERS in CMB anisotropy maps. First of all, we assume that ERS follow a Poisson distribution in the sky. The contribution of clustered ERS to the angular power spectrum of CMB temperature anisotropy is in fact small and can be neglected, if ERS are not subtracted down to faint flux limits (the signal due to clustered ERS becomes more relevant only at relatively low fluxes, that is, $S < 10$ mJy, [75, 76]).

It is well known that an ensemble of Poisson distributed point sources gives rise to a flat power spectrum of temperature fluctuations [77]. For a sample of sources with flux density below some cut-off S_c, the amplitude of this white noise spectrum is given by

$$C_{T\ell} = \left(\frac{dB}{dT}\right)^{-2} N\langle S^2\rangle = \left(\frac{dB}{dT}\right)^{-2} \int_0^{S_c} n(S) S^2 dS, \quad (5)$$

where N and $n(S)$ are, respectively, the total and the differential number of sources per steradian, and dB/dT is

Table 5: Expected total numbers of ERS with polarized intensity $\geq P_{\rm lim}$ over the full sky at *Planck* frequencies. For each *Planck* channel, the minimum and maximum values here indicated refer to our predictions calculated by the more "optimistic" and by the more "conservative" cases previously discussed (see Table 4).

$P_{\rm lim}$	ν [GHz]						
[mJY]	30	44	70	100	143	217	353
50	107–164	91–140	98–151	83–129	71–109	59–89	47–70
80	49–77	42–66	47–74	41–64	35–55	30–46	25–37
100	34–53	29–46	33–52	**28–45**	**25–39**	**21–33**	**18–27**
200	**10–16**	9–14	10–16	9–15	8–13	7–12	6–10
300	5–7	**4–7**	**5–8**	4–7	4–7	4–6	3–5
400	3-4	2–4	3–5	3-4	2–4	2–4	2-3
WMAP[1]	8	6	4				

[1]Number of polarized ERS detected in the WMAP 5 yr data at $|b| > 5^\circ$ by [55] at 33, 41 and 61 GHz ($P_{\rm lim} \approx 300$ mJy).

the conversion factor from brightness to temperature, that is, $dB/{\rm d}T \approx 10^{-2}\,\mu{\rm K}/({\rm Jy\,sr^{-1}})(e^x - 1)^2/(x^4 e^x)$ and $x = \nu/56.8\,{\rm GHz}$.

As an analogy to the expression of the angular power spectrum in total intensity or CMB temperature, it is possible to define the angular power spectrum for the Stokes parameters Q and U. Because point sources contribute, on average, equally to Q, U and to the E-, B-mode power spectra, we assume $C_{E\ell} \simeq C_{B\ell} \simeq C_{Q\ell} \simeq C_{U\ell}$ (we generally refer to them as polarization spectra). Following the treatment given by [16], we have that

$$\begin{aligned} C_{Q\ell} &= \left(\frac{dB}{dT}\right)^{-2} N\langle Q^2\rangle \\ &= \left(\frac{dB}{dT}\right)^{-2} N\langle S^2\Pi^2\cos^2(2\phi)\rangle \\ &= \left(\frac{dB}{dT}\right)^{-2} N\langle S^2\rangle\langle\Pi^2\rangle\langle\cos^2(2\phi)\rangle \\ &= \frac{1}{2}\left(\frac{dB}{dT}\right)^{-2}\langle\Pi^2\rangle C_{T\ell}, \end{aligned} \tag{6}$$

where the Stokes parameter Q is written in terms of Π and of the polarization angle in the chosen reference system, ϕ. The factor 1/2 arises because of the uniform distribution of polarization angles. It is easy to demonstrate that the cross-correlation temperature-polarization spectra are null, for example, $C_{TQ\ell} = \langle S^2\Pi\cos(2\phi)\rangle = 0$.

In (3) and (6) we have assumed that the fractional polarization is independent of the total intensity of the source. Observations for flat-spectrum sources in the flux density range $S \gtrsim 100$ mJy seem to support this assumption (see Section 4.1). We expect that this is maintained also at fainter fluxes but only if FSRQs and BL Lacs are separated into two different populations. On the other hand, this hypothesis may not be true for steep-spectrum sources: a clear anticorrelation between Π and S is observed from data at 1.4 GHz, whereas, at higher frequencies, the lack of large samples of steep-spectrum sources does not allow to determine it. In any case, steep-spectrum ERS are giving a negligible contribution to number counts at $\nu \geq 100$ GHz and, thus, this lack of information does not affect our current predictions.

In Figure 7 we present the results on ERS polarization power spectra for the six *Planck* frequencies where ERS are relevant. The value of $\langle\Pi^2\rangle^{1/2}$ is taken according to Table 4 for the different radio source populations. Moreover, we consider two cutoffs in flux density: $S_c = 1$, and 0.1 Jy. The former value is close to the completeness limit obtained by the *Planck* ERSCS for the frequency channels $\nu \leq 100$ GHz [59]; the latter one can be seen as a (somewhat optimistic) reference value for the *Planck* high frequency channels, or a reference value for future experiments.

In Figure 7 we also plot the CMB power spectrum for the E-mode and for the B-mode with a tensor-to-scalar ratio $r = 0.1$, 0.01 and 0.001. In this way we can have an indication of the level of ERS subtraction required to allow the detection of a gravitational wave induced primordial CMB B-mode signal. ERS should not be a strong constraint on detecting E-mode polarization or the B-modes with $r \gtrsim 0.01$. On the other hand, a primordial CMB B-mode signal corresponding to lower r values requires the subtraction of ERS down to flux detection limits of ~100 mJy, which will not be easy, or even possible, with the *Planck* sensitivity.

7. Conclusions

In this contribution we have reviewed recently available polarimetric surveys of extragalactic radio sources at frequencies $\nu \gtrsim 1$ GHz. These data point out that the typical intrinsic fractional polarization of ERS is around 2–5% of the total flux density, S, of the source even at frequencies as high as 20 GHz, and that in very few objects the fractional polarization is $\Pi \gtrsim 10\%$. This may be due to the low degree of uniformity of magnetic fields in the internal part of AGN jets and in lobes. Faraday depolarization is probably the cause of the large number of sources with a very low level of polarization, that is, $\Pi \lesssim 1\%$, at GHz frequencies, which also explains the strong increase of the fractional polarization observed at $\nu \gtrsim 10$ GHz in those objects. This conclusion is supported by high or extreme values of rotation measure RM $\gg 1000\,{\rm rad\,m^{-2}}$ observed in some blazars (e.g., [37, 39]).

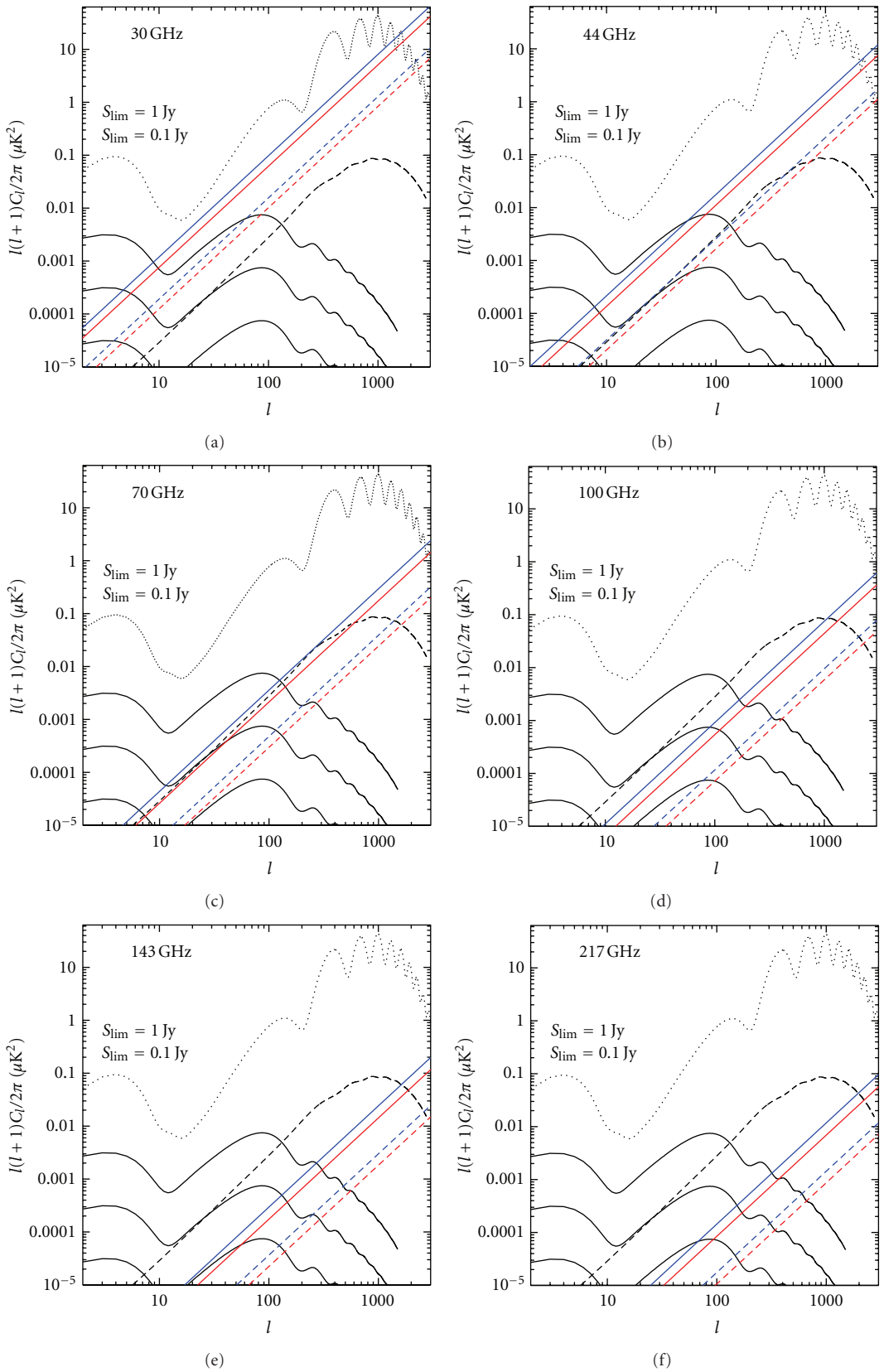

Figure 7: Polarization power spectra at six *Planck* frequencies for the CMB radiation (black lines: dotted lines for the E-mode; solid lines for the gravitational wave B-mode with $r = 0.1$, 0.01 and 0.001; dashed lines for the lensing-induced B-mode) and for ERS (solid lines are for $S_c = 1$ Jy and dashed lines for $S_c = 0.1$ Jy; blue lines correspond to the more "conservative" case and red lines to the more "optimistic" case).

Moreover, we have studied how polarization properties of ERS change from cm to mm wavelengths. For flat-spectrum sources a weak but constant increase of fractional polarization is observed, with median (mean) values varying from 1.5% (2–2.5%) at 1.4 GHz, to 2–2.5% (2.5–3%) at 5–10 GHz and 2-3% (3–3.5%) at 10–40 GHz. Indications that fractional polarization in blazars could further increase above 40 GHz come from the recent works by [39, 49]. On the other hand, a significantly higher fractional polarization is typically found in steep-spectrum sources, especially at high frequencies (median is 4-5% at 10–20 GHz and mean between 5 and 6.5%). However, because of incompleteness of the samples and of the small number of steep-spectrum sources in surveys at $\nu \gtrsim 10$ GHz, current observations could be biased by high-polarized objects.

In general, we do not find any dependence of the fractional polarization of ERS with the flux density at high radio frequencies. However, more conclusive evidences require larger and deeper surveys. Nevertheless, an anticorrelation between Π and S in blazars is expected when very faint flux densities are considered (see Section 4). For the flux-density ranges covered by available surveys, flat-spectrum sources are dominated by quasars (FSRQs). These objects are typically less polarized than BL Lacs [49], which become increasingly relevant at fainter flux densities and become the dominant population at $S \lesssim 10$ mJy [18, 78].

We also discuss a formalism to estimate ERS number counts in polarization and to predict the contribution of unresolved ERS to angular power spectra at CMB frequencies. As a first application, we attempt to predict how many polarized ERS the *Planck* Satellite will be able to detect in the different channels sensible to polarization measurements: we expect that only a dozen polarized ERS could be detected by *Planck* LFI, and a few tens at the HFI frequencies. Although the number of *Planck* detected sources is low, these data will allow us to study the frequency dependence of the fractional polarization in a wide range of frequencies, from 30 to 353 GHz, thus providing original and valuable information on polarization properties of ERS in the innermost regions of AGN jets.

Finally, our results on polarization power spectra demonstrate that ERS should not be a strong contaminant to the CMB E-mode polarization when observing at frequencies $\nu \gtrsim 70$ GHz. Moreover, it seems unlikely that ERS will have a significant impact on our ability to detect the B-mode polarization from primordial graviational waves if $r > 0.01$. On the contrary, if the cosmological B-mode signal is fainter, some strategy will be required to subtract the confusion noise produced by radio sources with flux-density $S < 1$ Jy. At sub-mm wavelengths, where radio sources become less and less relevant, confusion noise of point sources may be dominated by dusty galaxies (e.g., [79]). Polarization of these objects should be relatively low, but they are expected to be significantly clustered. Although the level of this effect is still quite uncertain, polarization spectra from dusty galaxies could begin to dominate the one produced by ERS already at $\nu \gtrsim 200$–300 GHz, at least at angular scales relevant for the detection of the B-modes.

Acknowledgments

The authors thank the referee, R. B. Partridge, for his insightful comments and criticisms that helped a lot in clarifying the main assumptions of the paper and also in improving its final presentation. M. Tucci acknowledges financial support from the French "Centre National d' Études Spatiales" (CNES). L. Toffolatti acknowledges partial financial support from the Spanish Ministry of Science and Innovation (MICINN), under project AYA2010-21766-C03-01.

References

[1] V. L. Ginzburg and S. I. Syrovatski, "Cosmic Magnetobremsstrahlung (synchrotron Radiation)," *Annual Review of Astronomy & Astrophysics*, vol. 3, pp. 297–350, 1965.

[2] V. L. Ginzburg and S. I. Syrovatski, "Developments in the theory of synchrotron radiation and its reabsorption," *Annual Review of Astronomy & Astrophysics*, vol. 7, pp. 375–420, 1969.

[3] A. R. Taylor, J. M. Stil, J. K. Grant et al., "Radio polarimetry of the ELAIS N1 field: polarized compact sources," *The Astrophysical Journal*, vol. 666, p. 201, 2007.

[4] T. Murphy, E. M. Sadler, R. D. Ekers et al., "The Australia Telescope 20 GHz survey: the source catalogue," *Monthly Notices of the Royal Astronomical Society*, vol. 402, no. 4, pp. 2403–2423, 2010.

[5] J. M. Kovac, E. M. Leitch, C. Pryke, J. E. Carlstrom, N. W. Halverson, and W. L. Holzapfel, "Detection of polarization in the cosmic microwave background using DASI," *Nature*, vol. 420, no. 6917, pp. 772–787, 2002.

[6] L. Page, G. Hinshaw, E. Komatsu et al., "Three-year Wilkinson Microwave Anisotropy Probe (WMAP) observations: polarization analysis," *The Astrophysical Journal Supplement Series*, vol. 170, no. 2, article 335, 2007.

[7] J. Dunkley, D. N. Spergel, E. Komatsu et al., "Five-year Wilkinson Microwave Anisotropy Probe (WMAP) observations: bayesian estimation of CMB polarization maps," *The Astrophysical Journal*, vol. 701, no. 2, pp. 1804–1813, 2009.

[8] M. Zaldarriaga and U. Seljak, "All-sky analysis of polarization in the microwave background," *Physical Review D*, vol. 55, no. 4, pp. 1830–1840, 1997.

[9] M. Kamionkowski, A. Kosowsky, and A. Stebbins, "Statistics of cosmic microwave background polarization," *Physical Review D*, vol. 55, no. 12, pp. 7368–7388, 1997.

[10] J. Tauber, N. Mandolesi, J.-L. Puget et al., "*Planck* pre-launch status: the *Planck* mission," *Astronomy & Astrophysics*, vol. 520, article A1, 2010.

[11] Planck Collaboration, "*Planck* early results. I. The *Planck* mission," *Astronomy & Astrophysics*, vol. 536, article A1, 2011.

[12] J. P. Leahy, M. Bersanelli, O. D'Arcangelo et al., "*Planck* pre-launch status: expected LFI polarisation capability," *Astronomy & Astrophysics*, vol. 520, article A8, 2010.

[13] C. Rosset, M. Tristram, N. Ponthieu et al., "*Planck* pre-launch status: high frequency instrument polarization calibration," *Astronomy & Astrophysics*, vol. 520, article A13, 2010.

[14] G. Efstathiou and S. Gratton, "B-mode detection with an extended Planck mission," *Journal of Cosmology and Astroparticle Physics*, vol. 6, p. 11, 2009.

[15] The COrE Collaboration, C. Armitage-Caplan et al., "Cosmic origin explorer," a proposal submitted to ESA for the 2015–2025 Horizon Programme, 2011.

[16] M. Tucci, E. Martinez–Gonzalez, L. Toffolatti, J. Gonzalez-Nuevo, and G. De Zotti, "Predictions on the high-frequency polarization properties of extragalactic radio sources and implications for polarization measurements of the cosmic microwave background," *Monthly Notices of the Royal Astronomical Society*, vol. 349, no. 4, pp. 1267–1277, 2004.

[17] L. Toffolatti, F. Argueso, G. De Zotti et al., "Extragalactic source counts and contributions to the anisotropies of the cosmic microwave background: predictions for the *Planck* surveyor mission," *Monthly Notices of the Royal Astronomical Society*, vol. 297, no. 1, pp. 117–127, 1998.

[18] G. De Zotti, R. Ricci, D. Mesa et al., "Predictions for high-frequency radio surveys of extragalactic sources," *Astronomy & Astrophysics*, vol. 431, no. 3, pp. 893–903, 2005.

[19] M. Tucci, L. Toffolatti, G. De Zotti, and E. Martinez-Gonzalez, "High-frequency predictions for number counts and spectral properties of extragalactic radio sources. New evidence of a break at mm wavelengths in spectra of bright blazar sources," *Astronomy & Astrophysics*, vol. 533, article A57, 2011.

[20] D. Mesa, C. Baccigalupi, G. De Zotti et al., "Polarization properties of extragalactic radio sources and their contribution to microwave polarization fluctuations," *Astronomy & Astrophysics*, vol. 396, no. 2, pp. 463–471, 2002.

[21] E. M. Sadler, R. Ricci, R. D. Ekers et al., "The properties of extragalactic radio sources selected at 20 GHz," *Monthly Notices of the Royal Astronomical Society*, vol. 371, no. 2, pp. 898–914, 2006.

[22] R. Subrahmanyan, R. D. Ekers, L. Saripalli, and E. M. Sadler, "ATLBS: the Australia telescope low-brightness survey," *Monthly Notices of the Royal Astronomical Society*, vol. 402, no. 4, pp. 2792–2806, 2010.

[23] J. K. Banfield, S. J. George, A. R. Taylor et al., "Polarized radio sources: a study of luminosity, redshift and infrared colors," *The Astrophysical Journal*, vol. 733, no. 1, article 69, 2011.

[24] H. Shi, H. Liang, J. L. Han, and R. W. Hunsted, "Radio source with ulttrahigh polarization," *Monthly Notices of the Royal Astronomical Society*, vol. 409, no. 2, pp. 821–838, 2010.

[25] M. Ruszkowski and M. C. Begelman, "Circular polarization from stochastic synchrotron sources," *Astrophysical Journal Letters*, vol. 573, no. 2 I, pp. 485–495, 2002.

[26] F. F. Gardner and J. B. Whiteoak, "The polarization of cosmic radio waves," *Annual Review of Astronomy & Astrophysics*, vol. 4, pp. 245–292, 1966.

[27] J. A. Hogbom, "A study of the radio galaxies 3C111, 192, 219, 223, 315 and 452," *Astronomy & Astrophysics Supplement Series*, vol. 36, pp. 173–192, 1979.

[28] R. A. Laing, "A model for the magnetic-field structure in extended radio sources," *Monthly Notices of the Royal Astronomical Society*, vol. 193, pp. 439–449, 1980.

[29] R. A. Laing, "Magnetic fields in extragalactic radio sources," *The Astrophysical Journal*, vol. 248, pp. 87–104, 1981.

[30] A. P. Marscher and W. K. Gear, "Models for high-frequency radio outbursts in extragalactic sources, with application to the early 1983 millimeter-to-infrared flare of 3C 273," *The Astrophysical Journal*, vol. 298, pp. 114–127, 1985.

[31] J. R. P. Angel and H. S. Stockman, "Optical and infrared polarization of active extragalactic objects," *Annual Review of Astronomy & Astrophysics*, vol. 18, pp. 321–361, 1980.

[32] T. Beckert and H. Falcke, "Circular polarization of radio emission from relativistic jets," *Astronomy & Astrophysics*, vol. 388, no. 3, pp. 1106–1119, 2002.

[33] D. P. Rayner, R. P. Norris, and R. J. Sault, "Radio circular polarization of active galaxies," *Monthly Notices of the Royal Astronomical Society*, vol. 319, no. 2, pp. 484–496, 2000.

[34] R. G. Strom, "Faraday depolarization of radio galaxies and quasars with simple spectra," *Astronomy & Astrophysics*, vol. 25, article 303, 1973.

[35] C. Burigana, L. La Porta, W. Reich et al., "Polarized synchrotron emission," in *Proceedings of the CMB and Physics of Early Universe*, pp. 20–22, Ischia, Italy, April 2006.

[36] B. F. C. Cooper and R. M. Price, "Faraday rotation effects associated with the radio source Centaurus A," *Nature*, vol. 195, no. 4846, pp. 1084–1085, 1962.

[37] R. T. Zavala and G. B. Taylor, "A View through Faraday's fog: parsec scale rotation measures in active galactic nuclei," *The Astrophysical Journal*, vol. 589, no. 1, article 126, 2003.

[38] R. T. Zavala and G. B. Taylor, "A view through Faraday's Fog 2: parsec scale rotation measures in 40 AGN," *The Astrophysical Journal*, vol. 612, no. 2, pp. 749–779, 2004.

[39] R. A. Battye, I. W. A. Browne, M. W. Peel, N. J. Jackson, and C. Dickinson, "Statistical properties of polarized radio sources at high frequency and their impact on cosmic microwave background polarization measurements," *Monthly Notices of the Royal Astronomical Society*, vol. 413, no. 1, pp. 132–148, 2011.

[40] A. R. Taylor, J. M. Stil, and C. Sunstrum, "A rotation measure image of the sky," *Astrophysical Journal Letters*, vol. 702, no. 2, pp. 1230–1236, 2009.

[41] J. J. Condon, W. D. Cotton, E. W. Greisen et al., "The NRAO VLA sky survey," *Astronomical Journal*, vol. 115, no. 5, pp. 1693–1716, 1998.

[42] P. C. Gregory, W. K. Scott, K. Douglas, and J. J. Condon, "The GB6 catalog of radio sources," *Astrophysical Journal Supplement*, vol. 103, pp. 427–432, 1996.

[43] J. K. Grant, A. R. Taylor, J. M. Stil et al., "The drao *Planck* deep fields: the polarization properties of radio galaxies at 1.4 GHz," *Astrophysical Journal Letters*, vol. 714, no. 2, pp. 1689–1701, 2010.

[44] M. Massardi, A. Bonaldi, M. Negrello, S. Ricciardi, A. Raccanelli, and G. de Zotti, "A model for the cosmological evolution of low-frequency radio sources," *Monthly Notices of the Royal Astronomical Society*, vol. 404, no. 1, pp. 532–544, 2010.

[45] M. Vigotti, G. Grueff, R. Perley, B. G. Clark, and A. J. Bridle, "Structures, spectral indexes, and optical identifications of radio sources selected from the B3 catalogue," *Astronomical Journal*, vol. 98, pp. 419–499, 1989.

[46] U. Klein, K. H. Mack, L. Gregorini, and M. Vigotti, "Multi-frequency study of the B3-VLA sample. III. Polarisation properties," *Astronomy & Astrophysics*, vol. 406, no. 2, pp. 579–592, 2003.

[47] M. Massardi, R. D. Ekers, T. Murphy et al., "The Australia Telescope 20 GHz (AT20G) survey: analysis of the extragalactic source sample," *Monthly Notices of the Royal Astronomical Society*, vol. 412, no. 1, pp. 318–330, 2011.

[48] N. Jackson, W. A. Browne, R. A. Battye, D. Gabudza, and A. C. Taylor, "High-frequency radio polarization measurements of *WMAP* point sources," *Monthly Notices of the Royal Astronomical Society*, vol. 401, no. 2, pp. 1388–1389, 2010.

[49] I. Agudo, C. Thum, H. Wiesemeyer, and T. P. Krichbaum, "A 3.5 mm polarimetric survey of radio-loud active galactic nuclei," *Astrophysical Journal, Supplement Series*, vol. 189, no. 1, pp. 1–14, 2010.

[50] A. Sajina, B. Partridge, T. Evans et al., "High-frequency radio spectral energy distributions and polarization fractions of sources in Atacama Cosmology Telescope survey field," *The Astrophysical Journal*, vol. 732, no. 1, article 45, 2011.

[51] R. Ricci, I. Prandoni, C. Gruppioni, R. J. Sault, and G. De Zotti, "High-frequency polarization properties of southern Kühr sources," *Astronomy & Astrophysics*, vol. 415, no. 2, pp. 549–558, 2004.

[52] H. Kuhr, A. Witzel, I. I. K. Pauliny-Toth, and U. Nauber, "A catalogue of extragalactic radio sources having flux densities greater than 1 Jy at 5 GHz," *Astronomy & Astrophysics*, vol. 45, pp. 367–430, 1981.

[53] T. Hovatta, E. Valtaoja, M. Tornikoski, and A. Lähteenmäki, "Doppler factors, Lorentz factors and viewing angles for quasars, BL Lacertae objects and radio galaxies," *Astronomy & Astrophysics*, vol. 494, no. 2, pp. 527–537, 2009.

[54] A. B. Pushkarev, Y. Y. Kovalev, M. L. Lister, and T. Savolainen, "Jet opening angles and gamma-ray brightness of AGN," *Astronomy & Astrophysics*, vol. 507, no. 2, pp. L33–L36, 2009.

[55] M. Lopez-Caniego, M. Massardi, J. Gonzalez–Nuevo et al., "Polarization of the *WMAP* point sources," *The Astrophysical Journal*, vol. 705, no. 1, artkicle 868, 2009.

[56] M. Lavalley, T. Isobe, and E. Feigelson, "ASURV: astronomy survival analysis package," in *Proceedings of the Astronomical Data Analysis Software and Systems I, A.S.P. Conference Series*, D. M. Worrall, C. Biemesderfer, and J. Barnes, Eds., vol. 25, p. 245, 1992.

[57] J. D. Vieira, T. M. Crawford, E. R. Switzer et al., "Extragalactic millimeter-wave sources in South Pole Telescope survey data: source counts, catalog, and statistics for an 87 square-degree field," *The Astrophysical Journal*, vol. 719, no. 1, article 763, 2010.

[58] T. A. Marriage, J. B. Juin, Y.-T. Lin et al., "The Atacama Cosmology telescope: extragalactic sources at 148 GHz in the 2008 survey," *The Astrophysical Journal*, vol. 731, no. 2, article 100, 2011.

[59] Planck Collaboration, "*Planck* Early results. XIII. Statistical properties of extragalactic radio sources in the *Planck* early release compact source catalogue," *Astronomy & Astrophysics*, vol. 536, article A13, 2011.

[60] L. Danese, A. Franceschini, L. Toffolatti, and G. De Zotti, "Interpretation of deep counts of radio sources," *The Astrophysical Journal*, vol. 318, pp. L15–L20, 1987.

[61] J. S. Dunlop and J. A. Peacock, "The redshift cut-off in the luminosity function of radio galaxies and quasars," *Monthly Notices of the Royal Astronomical Society*, vol. 247, no. 1, article 19, 1990.

[62] C. A. Jackson and J. V. Wall, "Extragalactic radio-source evolution under the dual-population unification scheme," *Monthly Notices of the Royal Astronomical Society*, vol. 304, no. 1, pp. 160–174, 1999.

[63] M. Tucci, J. A. Rubino-Martin, R. Rebolo et al., "Multifrequency spectral analysis of extragalactic radio sources in the 33-GHz VSA catalogue: sources with flattening and upturn spectrum," *Monthly Notices of the Royal Astronomical Society*, vol. 386, no. 3, pp. 1729–1738, 2008.

[64] K. I. Kellermann, "On the interpretation of radio-source spectra and the evolution of radio galaxies and quasi-stellar sources," *The Astrophysical Journal*, vol. 146, article 621, 1966.

[65] R. D. Blandford and A. Konigl, "Relativistic jets as compact radio sources," *The Astrophysical Journal*, vol. 232, pp. 34–48, 1979.

[66] Planck Collaboration, "*Planck* early results. XV. Spectral energy distributions and radio continuum spectra of northern extragalactic radio sources," *Astronomy & Astrophysics*, vol. 536, article A15, 2011.

[67] E. M. Waldram, R. C. Bolton, G. G. Pooley, and J. M. Riley, "Some estimates of the source counts at *Planck* Surveyor frequencies, using the 9C survey at 15 GHz," *Monthly Notices of the Royal Astronomical Society*, vol. 379, no. 4, pp. 1442–1452, 2007.

[68] J. Gonzalez-Nuevo, M. Massardi, F. Argueso et al., "Statistical properties of extragalactic sources in the New Extragalactic *WMAP* Point Source (NEWPS) catalogue," *Monthly Notices of the Royal Astronomical Society*, vol. 384, no. 2, pp. 711–718, 2008.

[69] M. Massardi, A. Bonaldi, L. Bonavera et al., "The *Planck*-ATCA Co-eval observations project: the bright sample," *Monthly Notices of the Royal Astronomical Society*, vol. 415, no. 2, pp. 1597–1610, 2011.

[70] A. Konigl, "Relativistic jets as X-ray and gamma-ray sources," *The Astrophysical Journal*, vol. 243, pp. 700–709, 1981.

[71] P. Giommi, G. Polenta, A. Lahteenmaki et al., "Simultaneous *Planck*, Swift, and Fermi observations of X-ray and gamma-ray selected blazars," *Astronomy & Astrophysics*. In press. http://arxiv.org/abs/1108.1114.

[72] D. Herranz, F. Argueso, and P. Carvalho, "Compact source detection in multi-channel microwave surveys: from SZ clusters to polarized sources," *Advances in Astronomy*. In press. Astrophysical Foregrounds in Microwave Surveys.

[73] U. Seljak, "Measuring polarization in the cosmic microwave background," *Astrophysical Journal Letters*, vol. 482, no. 1, pp. 6–16, 1997.

[74] M. Tucci, E. Martinez-Gonzalez, P. Vielva, and J. Delabrouille, "Limits on the detectability of the CMB B-mode polarization imposed by foregrounds," *Monthly Notices of the Royal Astronomical Society*, vol. 360, no. 3, pp. 935–949, 2005.

[75] J. Gonzalez-Nuevo, L. Toffolatti, and F. Argueso, "Predictions of the angular power spectrum of clustered extragalactic point sources at cosmic microwave background frequencies from flat and all-sky two-dimensional simulations," *The Astrophysical Journal*, vol. 621, no. 1, article 1, 2005.

[76] L. Toffolatti, M. Negrello, J. Gonzalez-Nuevo et al., "Extragalactic source contributions to arcminute-scale cosmic microwave background anisotropies," *Astronomy & Astrophysics*, vol. 438, no. 2, pp. 475–480, 2005.

[77] M. Tegmark and G. Efstathiou, "A method for subtracting foregrounds from multifrequency CMB sky maps," *Monthly Notices of the Royal Astronomical Society*, vol. 281, no. 4, pp. 1297–1314, 1996.

[78] P. Padovani, P. Giommi, H. Landt, and E. S. Perlman, "The deep x-ray radio blazar survey. III. radio number counts, evolutionary properties, and luminosity function of blazars," *The Astrophysical Journal*, vol. 662, no. 1 I, pp. 182–198, 2007.

[79] M. Negrello, F. Perrotta, J. Gonzalez-Nuevo et al., "Astrophysical and cosmological information from large-scale submillimetre surveys of extragalactic sources," *Monthly Notices of the Royal Astronomical Society*, vol. 377, no. 4, pp. 1557–1568, 2007.